Laser-Assisted Strain Engineering of Thin Elastomer Films to Form Variable Wavy Substrates for Cell Culture

Caterina Tomba, Tatiana Petithory, Riccardo Pedron, Aissam Airoudj, Ilaria Di Meglio, Aurelien Roux, Valeriy Luchnikov

▶ **To cite this version:**

Caterina Tomba, Tatiana Petithory, Riccardo Pedron, Aissam Airoudj, Ilaria Di Meglio, et al.. Laser-Assisted Strain Engineering of Thin Elastomer Films to Form Variable Wavy Substrates for Cell Culture. Small, 2019, 15 (21), pp.1900162. 10.1002/smll.201900162 . hal-02379017

HAL Id: hal-02379017
https://hal.science/hal-02379017

Submitted on 25 Jan 2023

HAL is a multi-disciplinary open access archive for the deposit and dissemination of scientific research documents, whether they are published or not. The documents may come from teaching and research institutions in France or abroad, or from public or private research centers.

L'archive ouverte pluridisciplinaire **HAL**, est destinée au dépôt et à la diffusion de documents scientifiques de niveau recherche, publiés ou non, émanant des établissements d'enseignement et de recherche français ou étrangers, des laboratoires publics ou privés.

Laser-assisted strain engineering of thin elastomer films to form variable wavy substrates for cell culture.

Caterina Tomba, Tatiana Petithory, Riccardo Pedron, Aissam Airoudj, Ilaria Di Meglio, Aurélien Roux, Valeriy Luchnikov**

C. Tomba
Department of Biochemistry, University of Geneva, quai Ernest Ansermet 30, CH-1211, Geneva, Switzerland
E-mail: caterina.tomba@unige.ch

T. Petithory
Institut de Science des Matériaux de Mulhouse, CNRS UMR 7361, 15, rue Jean Starcky, BP 2488, 68057 Mulhouse cedex France
Email: tatiana.petithory@uha.fr

R. Pedron
Institut de Science des Matériaux de Mulhouse, CNRS UMR 7361, 15, rue Jean Starcky, BP 2488, 68057 Mulhouse cedex France
The University of Strasbourg, Faculty of Pharmacy, 74 Route du Rhin, 67400 Illkirch-Graffenstaden, Strasbourg, France
Email: rpedron@unistra.fr

A. Airoudj
Institut de Science des Matériaux de Mulhouse, CNRS UMR 7361, 15, rue Jean Starcky, BP 2488, 68057 Mulhouse cedex France
Email: aissam.airoudj@uha.fr

I. Di Meglio
Department of Biochemistry, University of Geneva, quai Ernest Ansermet 30, CH-1211, Geneva, Switzerland
E-mail: ilaria.dimeglio@unige.ch

A. Roux
Department of Biochemistry and National Center of Competence in Research Chemical Biology, University of Geneva, quai Ernest Ansermet 30, CH-1211, Geneva, Switzerland
E-mail: aurelien.roux@unige.ch

V. Luchnikov
Institut de Science des Matériaux de Mulhouse, CNRS UMR 7361, 15, rue Jean Starcky, BP 2488, 68057 Mulhouse cedex FRANCE
Email: valeriy.luchnikov@uha.fr

Endothelial and epithelial cells usually grow on a curved environment, at the surface of organs, which many techniques have tried to reproduce. Here a simple method is proposed to control curvature of the substrate. Prestrained thin elastomer films are treated by infrared laser irradiation in order to rigidify the surface of the film. Wrinkled morphologies are produced upon stress relaxation for irradiation doses above a critical value. Wrinkle wavelength and depth are controlled by the prestrain, the laser power, and the speed at which the laser scans the film surface. Stretching of elastomer substrates with a "sand clock"-width profile enables the generation of a stress gradient, which results in patterns of wrinkles with a depth gradient. Thus, different combinations of topography changes on the same substrate can be generated. The wavelength and the depth of the wrinkles, which have the characteristic values within a range of several tens of µm, can be dynamically regulated by the substrate reversible stretching. It is shown that these anisotropic features are efficient substrates to control polarization of cell shapes and orientation of their migration. With this approach a flexible tool is provided for a wide range of applications in cell biophysics studies.

1. Introduction

During the past decades, living cell sensitivity to physical properties of their environment, such as nano- and microtopography, has been well established.[1,2] However, simple technologies that allow recapitulating in vitro the geometrical and highly dynamic properties of such multiscale structured environment are still lacking. Nevertheless, mimicking the physiological curvatures that characterize the in vivo environment is crucial to unravel biological and mechanical mechanisms modulated by geometrical confinement. In particular, recent efforts have been done to investigate the adaptation of cells and of nuclei to external mechanical properties,[3] in the reciprocal regulation of their shape and functions (e.g., by anisotropic compressive forces or homogeneous curvatures[4,5]). These studies support the more and more emergence of a direct mechanical continuity between the cytoskeleton

and the nucleoskeleton, which has great significance for its intrinsically participation in cell differentiation and fate, gene expression, mechanical response to force, and pathogenic mutations.[6–8]

In order to control shapes in nano- and microscale fabrication, gradients of mechanical stresses in thin films have become a rapidly growing field of research in the past few decades. Such gradients may have different origins, like the misfit of crystal lattice in the epitaxially grown multilayer semiconductor heterostructures[9] or selective swelling of components of multilayer polymer films.[10,11] These stress gradients are attractive because their relaxation causes film deformations, such as film rolling, wrinkling, or combination of these phenomena.[12] Wrinkled patterns often appear when a thin hard layer is created on an elastic, prestretched substrate. Relaxation of tensile strain of the substrate gives rise to the undulation of the thin "skin" layer, whose amplitude and wavelength are determined by the compromise between the bending energy of the hard layer, and the stretching energy of the substrate. One possible method is to fabricate polydimethylsiloxane (PDMS)/metal interfaces, such as gold layers. However, since gold has poor adhesiveness to PDMS, an intermediate titanium or chromium layer is required.[13] Therefore, multilayer depositions are required and the whole system consists of different materials, which can present limited stabilities in cell culture conditions (e.g., liquid medium).

Recently, spontaneously wrinkled substrates became a convenient tool for controlling living cell spreading and cytoskeletal arrangement on a sub-cellular scale roughness.[14–18] These wavy features present rounded edges that are inspired by in vivo nano- and microtopographies, allowing to different cell type manipulations. For example, bacterial biofilm growth reduction has been obtained on dynamic wrinkles with submicron to 2 μm valleys[19] and stem cell alignment and efficient internal organization for contraction have been shown on nano-scale wrinkles for tissue engineering applications.[20] However, these methods produce subcellular scaled surface features, which only partially recapitulate the complexity of curved environments in vivo. It is worth mentioning that apart of the cell growth control, the wrinkled morphologies are of essential interest in many other research fields such as the metrology of polymeric thin films,[21,22] adhesion control,[23] design of diffraction gratings,[24,25] and stretchable electronics.[12,26–28]

Recently, bigger concave or convex structures have also shown to guide cell orientation and migration.[5,29] However, the use of these curved substrates is still rare in biological studies. The flexibility of these methods is limited to the fabrication of a mold and abrupt angles are often present at the edges of the structures.[29,30]

In this study, we present how laser irradiation of a thin elastomer generates various curvatures of the substrate in a wide range of wavelengths and depths of the depression, which is comparable to the cell or multicell scale. This technique is applied as a tool to form anisotropic and actively deformable substrates for the study of cell orientation and motility. For this purpose, the application of mid-infrared ($\lambda = 10.8$ μm) laser irradiation is explored to hardening the surface of prestrained elastomer PDMS films. Micro- and macroscale deformations, which arise in course of the stress relaxation, are characterized as a function of the irradiation dose and the prestrain degree. By controlling the stretching rate or the elastomer shape, we tune the topographic parameters in time or with depth gradients on the same substrate.

This method could be a promising approach for further applications in cell culture. Indeed, it allows getting out-of-plane deformations comparable or larger than the cell size, in a simplified, flexible and cheap process: i) it requires only one step of fabrication (i.e., any mold or multilayer deposition are used), and ii) the parameters of the features are robustly controlled by the fabrication conditions (FCs) as well as being dynamically changed after cell deposition.

2. Wrinkled Morphologies

Our experimental setup is shown in Figure 1a. PDMS film (0.5 mm thick) is attached to a homemade stretcher and uniaxially elongated by 100% of its initial length. After that, the film is exposed to laser irradiation. The irradiation dose was tuned using the parameters: i) the laser pulse energy, ii) the speed of sample scanning by the laser, and iii) the number of times the sample was scanned by the laser. The parameters (i) and (ii) below are indicated by percentage from the maximal values, 35 W and 254 cm s−1 (in the raster mode) respectively. After irradiation, the film is slowly relaxed to 0% elongation state, before unmounting. Below, the FC is encoded as follows: P/V/N/S, where P is for laser power, V is for laser scan velocity, N is for number of scans, and S is for the stretching degree. If irradiation power is too high, the polymer burns and is torn apart, while if it is too low, wrinkles do not form. The range of suitable parameters for the wrinkle formation was found experimentally (Figure 1b). It should be noted that wrinkling is always accompanied by out-of-plane deformation of the films, while the inverse is not always true. Indeed, out-of-plane deformation is possible without the wrinkle formation.[12,26]

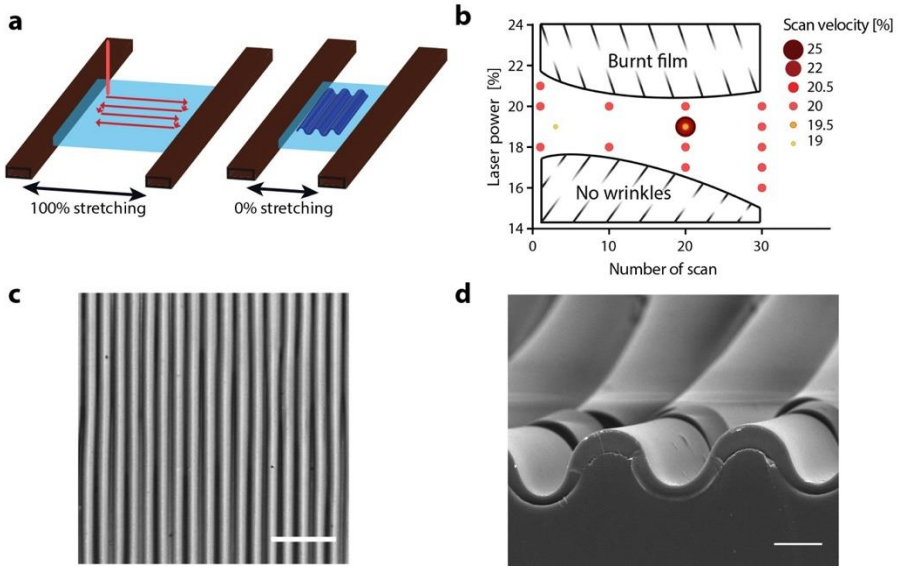

Figure 1. Wrinkled morphologies of a laser-treated PDMS film. a) Schematic layout of the experimental setup. b) Laser parameters of the irradiation dose: laser power (%), number of scans and scan velocity (circle size and color intensity are proportional to the % values). The suitable region for wrinkled patterns is delimited by the region where there is no wrinkle formation (below) or where the film burns (above). c) Optical microscopy image of a wrinkled film (top view). FC=18/20/10/100. Scale bar = 200 μm. d) SEM image of the film cross-section. FC=19/20/30/100. Scale bar = 50 μm.

Typical wrinkled morphologies, corresponding to two sets of FC, are shown in Figure 1c,d. The morphology shown in Figure 1c is practically defect less on the scale of 1 μm, and corresponds to a couple dozens of the wrinkle's wavelengths (λ = 50 μm). The high quality of the pattern can be attributed to slow strain release rate (<4 cm min^{-1}), which was found by Efimenko et al. to be a critical factor for the formation of defect-free wrinkles.[31] The formation of the wrinkled morphologies is usually related to the compression of a hard "skin" layer covering a relatively soft substrate. In order to elucidate the existence of such a skin layer, one of the samples was cut in the transversal direction. Its scanning electron microscope (SEM) image (Figure 1d) reveals clearly an interface between the laser-modified surface layer and the substrate. The SEM image of the substrate section also reveals the absence of abrupt angles, which guaranties a continuity in the substrate deformation.

Before the laser exposure, the film was shifted by 15 mm from the focal plane of the objective of the optical system of the laser (having the focal length F = 50.8 mm/2 in.) in order to obtain more mild conditions of the polymer irradiation. Indeed, the window suitable for wrinkle formation depends on the position of the film with respect to the focal plane of the lens in the laser optical system. As a result, at the typical scanning rate of 50.8 cm s^{-1} (20 in. s^{-1} or 20% of the maximal value), the burning threshold (the maximal laser power at which the polymer is not burned) shifted from ≈2.45 W (7% of the maximal value) to ≈7.7 W (22% of the maximal value). In our experimental setup, the irradiation dose received by the film per one scan at 20% of the maximal power and 20% of the maximal scan velocity (typical values for the present study) is equivalent to 23.1 J cm^{-2}. For multiple scans, the irradiation dose should be accordingly multiplied. Unfortunately, an accurate theoretical estimation of the temperature at the irradiation spot is not possible because of the uncertainty of the attenuation depth of the beam in the polymer, and the energy density distribution in the beam. In a future study, the direct measurements of the temperature at the irradiation spot will be done with the use of a fast infrared camera. However, shifting the film out of the beam focus allows also for more homogeneous irradiation of the film, due to a better overlapping of the regions irradiated by the consecutive laser pulses. Moreover, slightly defocusing the beam at the surface of the film allows for a broader range of FC parameters.

The dependence of the depth and the period (wavelength) of the wrinkles on the key fabrication parameters (laser power and the laser scan velocity) are shown in Figure 2a–d for different number of scans. Periodicities and depths of wrinkles were measured independently by confocal, digital, and electron microscopy; the results of the measurements are consistent between each technique. From these data we conclude that the wrinkle formation is much more sensitive to the laser power and the scan velocity, than to the number of scans. For instance, an increase of the laser power by two percent, from 18% to 20%, is equivalent to an increase of the scan number from 10 to 30. Analogously, the scan velocity increase by only 3%, from 19% to 22%, decreases the depth and the wavelength of the wrinkles more than twice.

Similar sensitivity of the morphologies to the laser power and the scan velocity was expected because the average power density transferred to the film is proportional to the ratio of these two FC parameters. These data indicate

that the irradiation effect is not determined by the total dose of energy transferred to the elastomer but rather strongly depends on the irradiation intensity. It is remarkable that the range of FC parameters corresponding to the formation of wrinkles in the relaxed samples is very narrow.

An eye-catching peculiarity of the wrinkles obtained for low relative irradiation intensity W = 18% (Figure 2e,i–iv) is their asymmetry with respect to top-down inversion. The wrinkles have nonsinusoidal shape, with the depressions degenerated in sharp folds. The wrinkles obtained by irradiation with W = 20%, but with the small number of scans (n = 2) belong also to this class of morphologies (Figure 2e,v). The degree of top-down asymmetry decreases for W = 20% with the number of scans (Figure 2e,vi–viii).

We first focused on the characterization of the most sinusoidal shaped wrinkles, where the skin layer at the surface of the substrate is clearly formed. Let us denote the surface layer and the substrate with the indices "sl" and "s." Thickness of this surface layer is h = 10 μm (FC = 20/20/20/100, Figure 2e,vii). The Young modulus of the material (E) was estimated locally by atomic force microscopy (AFM) (Peak-Force quantitative nanomechanical mapping mode; see Section S1 and Figures S1–S3, Supporting Information). For the sl, it decreased gradually from 152 Å} 11 MPa, for the region closest to the surface of the wrinkles, to 67 Å} 8 MPa at the sl/s interface. This is almost three orders of magnitude less than the Young modulus of silicon polymorphs.[32] The average value, Esl ≈ 112 MPa is taken into account below. For the untreated film far from the surface, the Young modulus, Es = 2 Å} 1 MPa, is about two orders of magnitude smaller than the modulus of the surface layer.

For the case of semi-infinite substrates, the formulas for the wrinkles wavelength and amplitude (defined as the half depth of the depression) are well known[33]

$$\lambda = 2\pi h \left(\frac{E_{sl}}{3E_s}\right)^{\frac{1}{3}} \quad (1)$$

$$A = h\sqrt{\frac{\varepsilon-\varepsilon_c}{\varepsilon_c}} \quad (2)$$

where ε_c is the critical strain,

$$\varepsilon_c = \frac{1}{4}\left(\frac{3E_s}{E_f}\right)^{\frac{2}{3}} \quad (3)$$

below which the wrinkles do not appear. For films with finite thickness, these formulas should be used with cautiousness, because the stress relaxation in the films is always accompanied by bending of the films. The bending can modify strongly the critical strain, as well as the amplitude and the wavelength of the wrinkles [12,34]. The period of wrinkles becomes independent of the substrate thickness *H* when the ratio between the bending stiffnesses of the superficial film and that of the substrate, $x = (E_{sl}h^3)/(E_sH^3)$, is less than 0.01 [34,35]. Application of this criterion to our system with the values E_{sl}, E_s and h given above, and the substrate thickness H = 500 μm gives $x = 4.6 \cdot 10^{-4}$ shows that the formulas (1-3) can be, in principle, applied to our system. Moreover, assuming that the irradiation does not significantly change the Poisson ratio of the material (ν), the factor $(1-\nu^2)^{-1}$, transforming the Young modulus to the plain-strain modulus, is canceled. Experimental values of the amplitude and the wavelength are compared with theoretical ones in Table 1.

	Experimental	Theoretical (for E_s = 2 MPa)	Theoretical (for E_s* = 6 MPa)
Wavelength (μm)	114 ± 8	240	115
Amplitude (μm)	22 ± 2	53	35

Table 1. Experimental and theoretically predicted values for the wavelength and the amplitude of the FC=20/20/20/100 sample (as shown in Figure 2e *vii*). Experimental values are reported from measurements by digital microscopy (wavelength, Figure 2c) and by confocal microscopy (amplitude of the sinusoidal shape, i.e. half depth of the depression, Figure 2a).

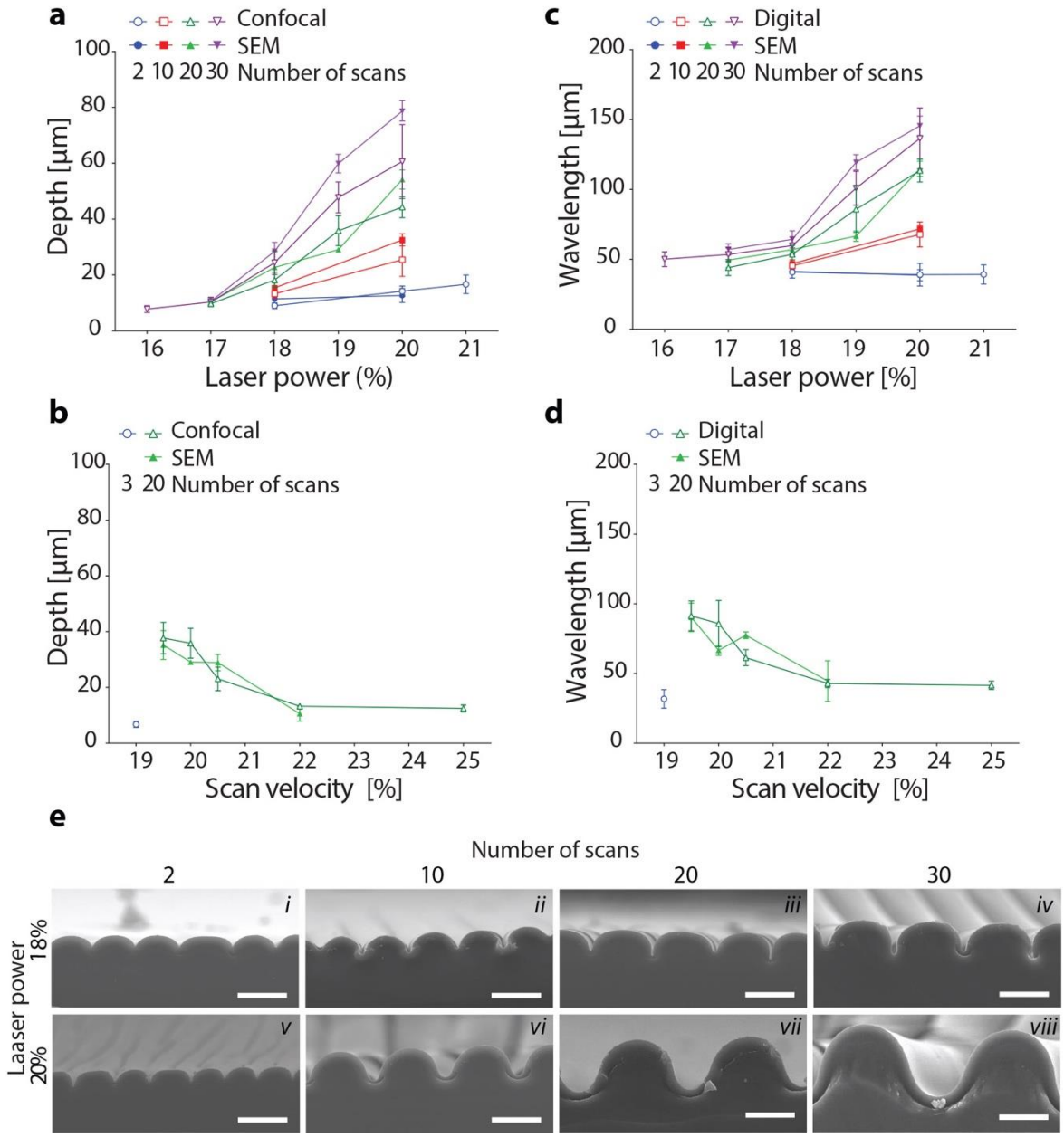

Figure 2. **Characterization of the wrinkled films.** a-b) Depth of the wrinkles as a function of the laser power (scan velocity = 20%) (a) and the laser scan velocity (laser power = 19%) (b). c-d) Wrinkle wavelength as a function of the laser power (scan velocity = 20%) (c) and the laser scan velocity (laser power = 19%) (d). e) SEM images of the wrinkle cross-section for different FC (scan velocity = 20%). Scale bars = 50 µm.

The large discrepancy between theoretical and experimental values can be explained partially by the uncertainty of the Young modulus measurements performed with AFM, whose accuracy depends on the roughness of the sample cut (see Section S1, Supporting Information). Also, despite the clear interface between the surface layer and the substrate, the latter is also irradiated by the laser to some extent. As a matter of fact, the Young modulus measured directly under the interface was $E_s^* \approx 6$ MPa, much larger than in the bulk part of the elastomer (2 MPa). If this higher modulus is used instead of 2 MPa in the formulas (1)–(3), the theoretical values for the wavelength and the amplitude are closer to the experimental ones (Table 1).

A more elaborated wrinkling theory, taking into account the gradients of mechanical properties, needs to be developed to fully explain our system.

Regarding the top-down asymmetry of wrinkles, it is a wellknown phenomenon which was reviewed by Brau et al.[36] It is attributed to the nonlinear (quadratic) term in the expression for normal force induced by the elastic foundation on the superficial rigid film. This term arises from the nonlinear relationship between the displacement vector and the strain tensor.[37] Theoretically, it is predicted to vanish for small wrinkling amplitudes. To verify this prediction, we have performed an additional experiment, in which a “sand clock”-shaped film was stretched (Figure 3a).

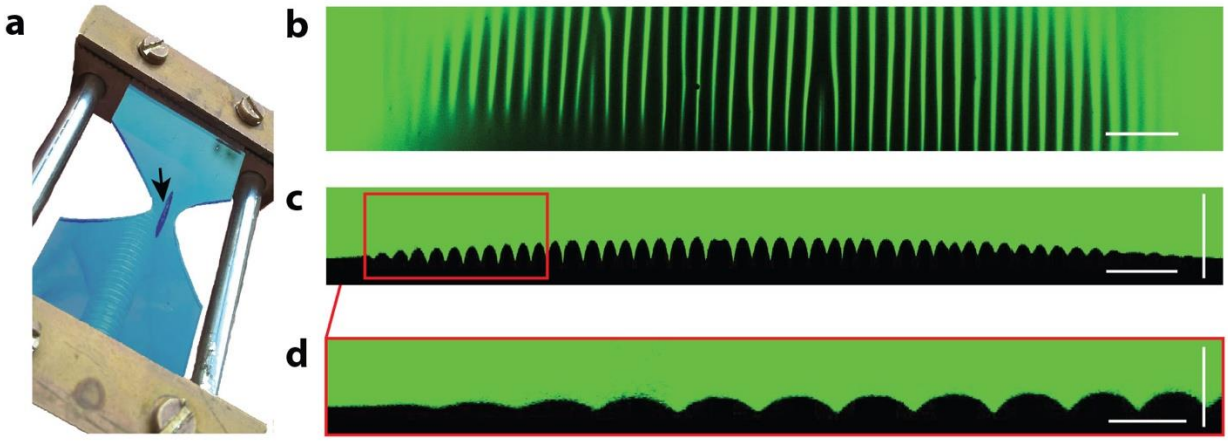

Figure 3. **Formation of wrinkles on an irradiated "sand clock"-shaped film.** a) A "sand clock"-shaped film on the stretching device. The black arrow points to the wrinkled area on the narrowest part of the stripe. FC = 20/20/10/50. b) Confocal image of 2 mm-long wrinkled area (top view, mid-plane of a z-stack). Scale bar = 200 µm. c) Cross-section showing the film profile (black) along the middle line of the wrinkled area. Horizontal bar = 200 µm. Vertical bar = 50 µm. d) Magnification of the left part of the profile. Horizontal bar = 100 µm. Vertical bar = 50 µm.

In this configuration, the degree of stretching is maximal for the middle of the film (see Figure S4a–d and Movie S1, Supporting Information, for a quantitative illustration of the film deformation). Wrinkled surface occupies an oval, a few millimeters long area at the neck of the film. The profile of the film along the long axis of this area was measured by confocal microscopy (Figure 3b).

As expected, the middle part of this area is occupied by the wrinkles of the largest depth, whose shape is characterized by a strong top-down asymmetry. Some wrinkles exhibit features of a period-doubling instability.[36] Surprisingly, the asymmetry persists also for wrinkles of vanishingly small depths, at the borders of the wrinkled area. Presently, we have no plausible explanation for this asymmetry in wrinkles of small depths. It may be related to the vertical gradient of Young modulus in irradiated film. The nonsinusoidal wrinkling was observed also by Fei et al.[38] in thin gold films on elastomeric substrates and was attributed to asymmetric behavior of the polycrystalline gold film when tension or compression are applied. By this approach that produces a strain gradient, we also estimated that a threshold of ≈65% of elongation appears like the minimum value of elastomer stretching to get wrinkle formation at the surface after relaxation (Figure S4e–g, Supporting Information).

3. Interaction of the Infrared Laser Irradiation with the PDMS Films

The stiffening of the elastomer upon irradiation described above suggests a structure evolution of the substrate surface. The mechanism behind this phenomenon has been investigated by ATR FT-IR (attenuated total reflection Fourier transform infrared) methods and Raman spectroscopy.

In several studies, indeed, it has been shown by Raman spectroscopy that the formation of Si-crystals is a consequence of irradiating the PDMS surface with different type of lasers.[39–41] Through their highly uniform bonds, these Si-crystals appear in a Raman analysis as a sharp peak with a characteristic strong band adjacent to the peaks of native PDMS.[40] However, in conditions used in this work to generate wrinkled patterns, the Raman spectra does not reveal the formation of any Si-crystals (Figure S5, Supporting Information). This result is consistent with images obtained by SEM, in which the surface of the film appears smooth (Figure 1d).

However, the IR spectra of an irradiated PDMS film (Figure 4a) highlights a remarkable change in shape of the absorption band between 950 and 1200 cm^{-1}, which is normally associated with the stretching vibrational modes of the Si-O-Si system. Indeed, PDMS usually produces a broad band split in two peaks,[42] which are clearly observable on the spectrum of the nonirradiated sample (peaks at 1020 and 1080 cm^{-1}). In contrast, on the spectra of the irradiated samples a single peak is observed at 1020 cm^{-1} with an important shoulder at 1100 cm^{-1}. These results show a strong alteration of the surface chemical bonds.

More precisely, the reduction of the ratio between the peak's area (Figure 4b), related to the methyl bending motions (rocking "ρ" vibrations at 740 cm^{-1} and symmetric bending "δs" vibrations at 1260 cm^{-1}) and the stretching motion "ν" of the siloxane group (in between 950 and 1200 cm^{-1}), suggests a reduction of the amount of methyl groups compared to the siloxane ones after irradiation. This evidence suggests that, as a consequence of the irradiation, an oxidation causes a deep modification of the backbone structure of the PDMS surface. This process is most probably also at the origin of the Young modulus increase observed by AFM: as hypothesized by Camino et al.,[43] the thermally induced oxidation could lead to further crosslinking of the polymer by the mechanism shown in Figure

4c, increasing its stiffness. Nevertheless, this mechanism does not exclude that further crosslinking due to radical formation also occurs (e.g., methylene or ethyl bridges between PDMS chains).[44]
In addition to the wrinkled morphologies, presented in the Section 2, laser irradiation of stretched elastomer films allows to obtain other interesting 3D structures.

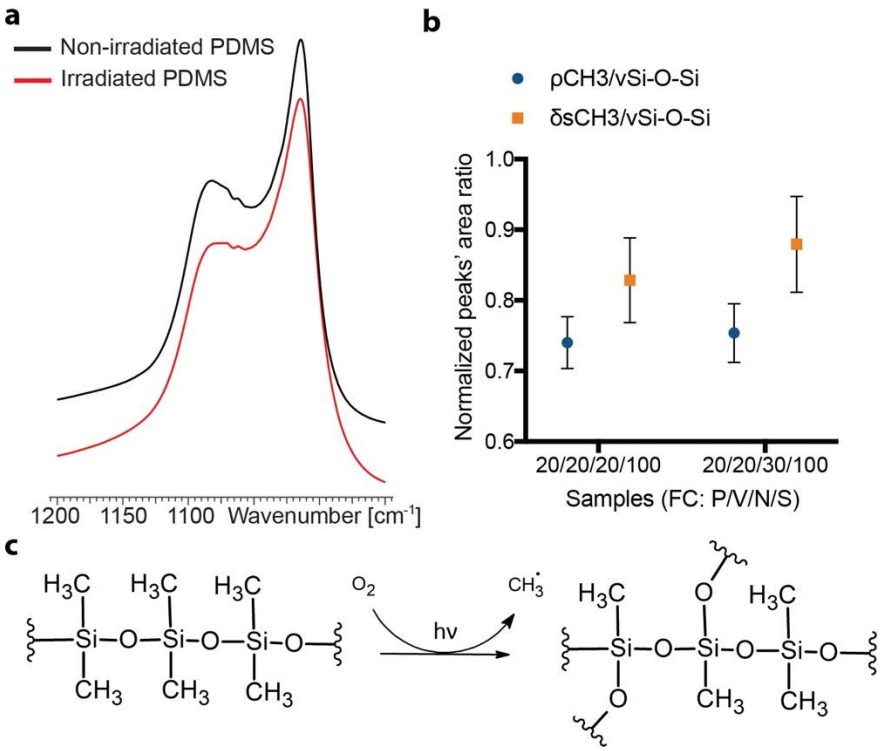

Figure 4. ATR-FTIR/Raman study of the effect of laser irradiation on the PDMS films. a) IR spectra of non-irradiated (black) and irradiated (red) samples. FC = 20/20/30/100. b) Ratio between the peak's area related to the methyl bending motions (●rocking "ρ" and ■ symmetric bending "δs" vibrations) and the stretching motion "ν" of the siloxane group, normalized for the one of the non-irradiated sample. FC = 20/20/20/100 and 20/20/30/100. c) Possible mechanism of crosslinking due to the oxidation of PDMS (adapted from [43]).

As mentioned in the Introduction, in case of substrates of finite thickness, wrinkling of the films is always accompanied by their bending.[12,26,34] Figure S6b in the Supporting Information shows two examples of the films, for the same relative laser power (18%) and scan velocity (20%), but for different numbers of the scans (5 and 10). Prior to irradiation, the films were stretched by 100%. The increase of scan number decreases the curvature radius from 6 to 2.5 mm, approximately; further increase of the scan number does not change the curvature radius significantly (data not shown). The curvature radius of the bilayer films is usually well captured by the classical Timoshenko formula.[45] However, it is unfortunately not applicable to our system because of the existence of the Young modulus gradients. As mentioned above, a future theory of the laser-irradiated elastomer films should take these gradients into account.
Another example of a 3D object that can be created by laser irradiation of strained elastomer films is a bistable structure, which can be obtained by consecutive irradiation of two opposite sides of the film, under perpendicular stretching directions. To that end, after the first irradiation of the stretched film, the film was relaxed, turned first by 90° around the normal axis, then by 180° around the horizontal axis collinear with the stretcher displacement direction, and irradiated again (see Figure S6a, Supporting Information, for the experimental setup). Figure S6c in the Supporting Information shows the two quasi-cylinder stable conformations obtained in the film. This kind of bistable films is well understood for laminates with anisotropic residual stress[46,47] and it is exploited in advanced applications such as soft and deployable actuators.[48] Further optimization and adaptation of these principles in order to reduce the size of these structures on microstructured elastic substrates may contribute to increase the possible configurations of cell microenvironments.

4. Application of the Wrinkled Surfaces as a Tool to Systematically Study Cell Response to Local and Anisotropic Curvature

Three different cell lines have been cultured on wrinkled substrates to probe the wide potential of this approach for cell

culture. The aim was to investigate the cell interaction with negative and positive curved substrates as well as the response to curvature changes. Due to the large microscale of the wrinkles, these structures are comparable to the cell size, allowing for cell shape deformation.

First, Hela cells were grown on "sand clock"-shaped films and their adaptation to unidirectional folds of the substrate was characterized. Their shape was quantified and then their mdisplacement was followed over time. According to the profile characterization of those substrates, three regions that lead to significantly different cell behaviors were identified (**Figure 5**a): flat film, the edges of the wrinkles (up to ≈5 µm of depth), and the central region of the wrinkles (up to ≈15 µm of depth). The profiles along the two perpendicular axes of the wrinkles are also reported, showing the regularity of both the wrinkled pattern and the gradual increase of wrinkle depth.

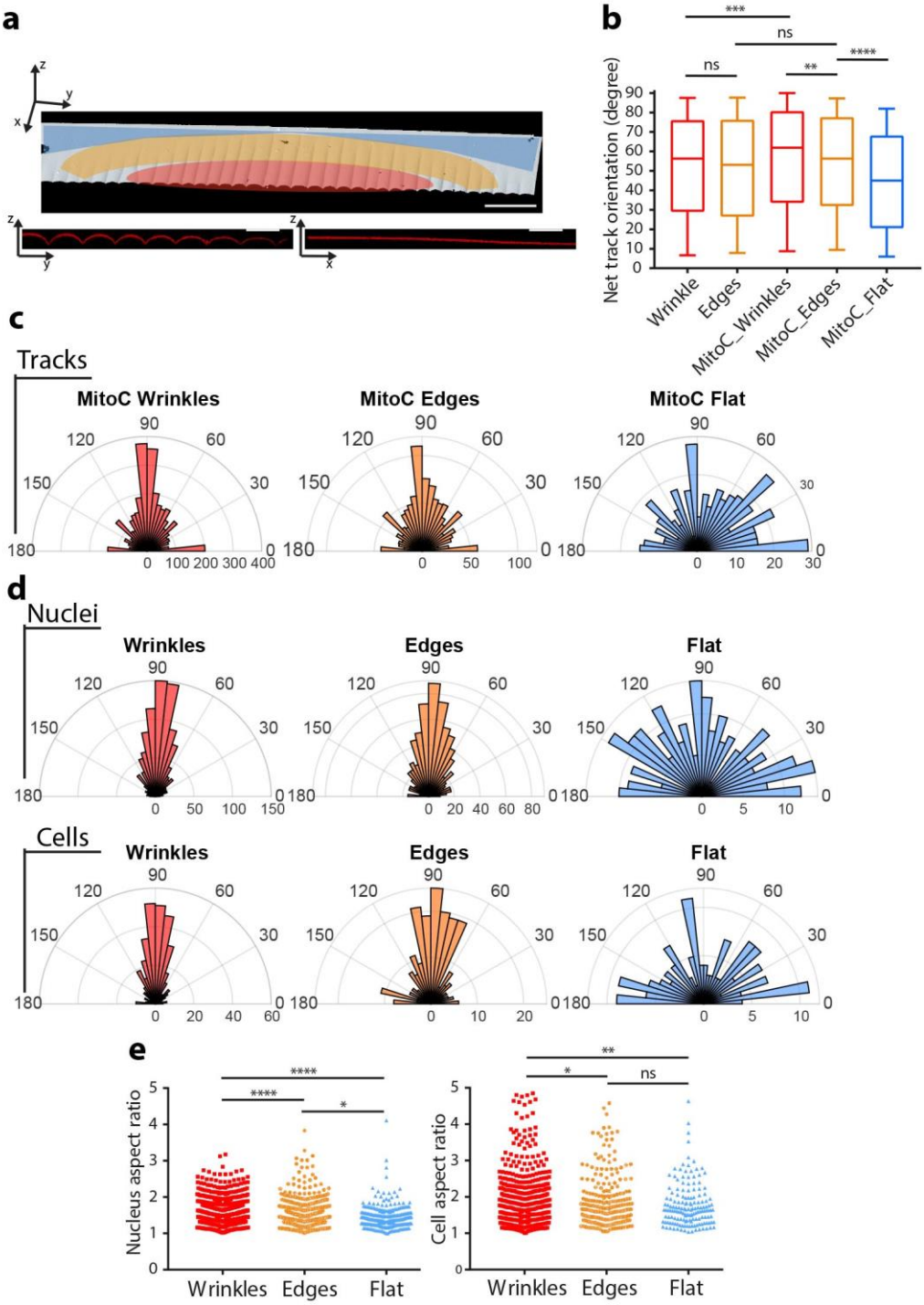

Figure 5. **Cell adaptation to wrinkled patterns on "sand clock"-shaped films.** a) Top: 3D reconstruction of a confocal z-stack of the PDMS film showing the 3 main regions: wrinkles (red), edges (orange) and flat (light blue). Scale bar = 200 µm. Bottom: cross-sections of the fluorescent fibronectin coating (red). Scale bars = 50 µm. b-c) Net track orientation of Hela cells on the 3 regions, without and with MitomycinC ("MitoC"). Box (b) and polar (c) plots (control, ns, p=0.3348, ****, p < 0.0001, n=1375, 562; MitoC, ns, p=0.0958, **, p=0.0052, ***, p= 0.0001,

****, $p < 0.0001$, n=3877, 1293, 448, Mann Whitney test). The value of 90 degrees corresponds to the x-axis in (a). Top and bottom of a box indicate 75th and 25th quartiles, respectively; whiskers indicate the min and the max values; the middle line is the median. d) Polar plots of the orientation of nuclei and Hela cells in the 3 regions. e) Distributions of the aspect ratio (longest/shortest axis) of nuclei and Hela cells (nuclei, *, p=0.0173, ****, $p < 0.0001$, n=866, 683, 266; cells, *, p=0.0139, **, p=0.0045, ns, p =5275, n=407, 237, 160, Mann Whitney test).

Within 12 h after cell spreading onto the substrate, an estimation of the nuclei positions indicates that cells migrate to valleys, as the valley-to-peak cell number ratio increased six times (data not shown). Furthermore, cells migrate preferentially along the wrinkles (Figure 5b,c and Figure S7, Supporting Information). Interestingly, blocking cell division by MitomycinC treatment enhances this directed motion. These experiments provide evidence that cells significantly align their migration direction with the wrinkle direction, after reaching a wrinkle (Figure 5d and Figure S8, Supporting Information). Moreover, cells and nuclei deform to adopt a polarized shape aligned with the wrinkle axis. Nuclei gradually become more anisotropic when the fold depth increases (from "edges" to "wrinkles" regions). Similarly, the cell aspect ratio (longest over shortest axis ratio) is higher on the central region ("wrinkles" region) of the patterned substrate (Figure 5e).

As reported above, both depth and wavelength of homogeneous wrinkles are timely modulated by unidirectional stretching. We observed that both properties can be varied of 100% of their initial value by modulating the stretching rate. Upon stretching of the film from 0% to 100%, cells adhering to curved films see the shape of the substrate to abruptly change from high to low curvature (**Figure 6**a). Moreover, by changing the wrinkled morphology, this method enables a modulation of lateral cell constrictions. Therefore, it results in a practical tool for further studies on cell adaptation to dynamic and anisotropic mechanical constraints.

In a reverse approach, homogeneous substrates remain flat after laser exposure, as long as stretching is not released, and upon which wrinkles appear on the surface. By taking advantage of this property, osteoblast cells were grown on flat films to qualitatively observe their response right after an abrupt change of curvature (Figure 6b). Interestingly, and according to the quantifications showed above, cells appear to transit from a homogeneously spread to an elongate shape in the valleys, where they longitudinally migrate. This result may lead to deeper studies of the mechanism understanding about cell migration and guidance in out-of-plane curved environments.

Finally, the application of this technique was explored to grow epithelial cells until confluency, demonstrating that this technique is also suitable for collective studies of cells, such as tissues. Indeed, Madin Darby canine kidney (MDCK) cells form a full and folded monolayer according to the initial wrinkle profile (when cells are seeded on nonstretched substrates, Figure 6c, top) and then deform in response to the elongation rate of the film (Figure S9, Supporting Information). Interestingly, at low rate of cell confluency (Figure 6c, left), the substrate surface is almost completely covered by spread cells, whereas nuclei are elongated and localized in the valleys. As clearly shown by the orthogonal views of the confocal z-stacks, they are then uniaxially deformed by stretching the PDMS film. As reported above, periodic stretching of the substrate would induce dynamic deformations of tissues, reproducing compression (Figure 6c, right) and tension processes similarly to the in vivo context.

Altogether, these results prove the potential of laser assisted strain engineering techniques to provide different, variable and reversible topographical parameters, with both negative and positive curvatures on the same substrate. Importantly, a homogeneous adhesive coating was attained, in order to guarantee the absence of artefacts due to the surface chemistry.

5. Conclusion

Hardening of prestrained PDMS films by mid-infrared irradiation is a promising approach for the fabrication of periodically undulated microstructured surfaces as well as 3D objects such as rolls and bistable structures. Irradiation above a threshold dose creates, on the surface of the elastomer, a rigid film of a few micrometers in thickness, whose Young modulus exceeds that of the untreated polymer by two orders of magnitude, while remaining two and a half orders of magnitude smaller than the Young modulus of silica polymorphs. Our approach is complementary to the recently reported near-infrared (λ = 1064 μm) treatment of prestrained PDMS[49] and permits obtaining wrinkles whose wavelengths and depths are one to two orders of magnitude larger than those obtained by Yu et al.[49] Remarkably, hardening of the film by mid-infrared radiation retains its flexibility, allowing for wrinkling and bending without cracks or silicon dioxide particles formation. Altogether, these properties illustrate the large benefit of this approach toward previously reported near-infrared laser irradiation, oxygen plasma treatment, or metallization of the elastomer.[20,49]

The irradiation dose is controlled with high precision by tuning the beam power, the scan velocity of the beam over the substrate, and the number of scans. These parameters control both the wavelength and the depth of the wrinkles, while the depth can be independently controlled by the prestrain of the stretched film. Indeed, gradients of strain in the samples were generated by stretching "sand clock"-shaped films. After irradiation, relaxation of the gradient strain resulted in wrinkled morphologies with a gradient of depths.

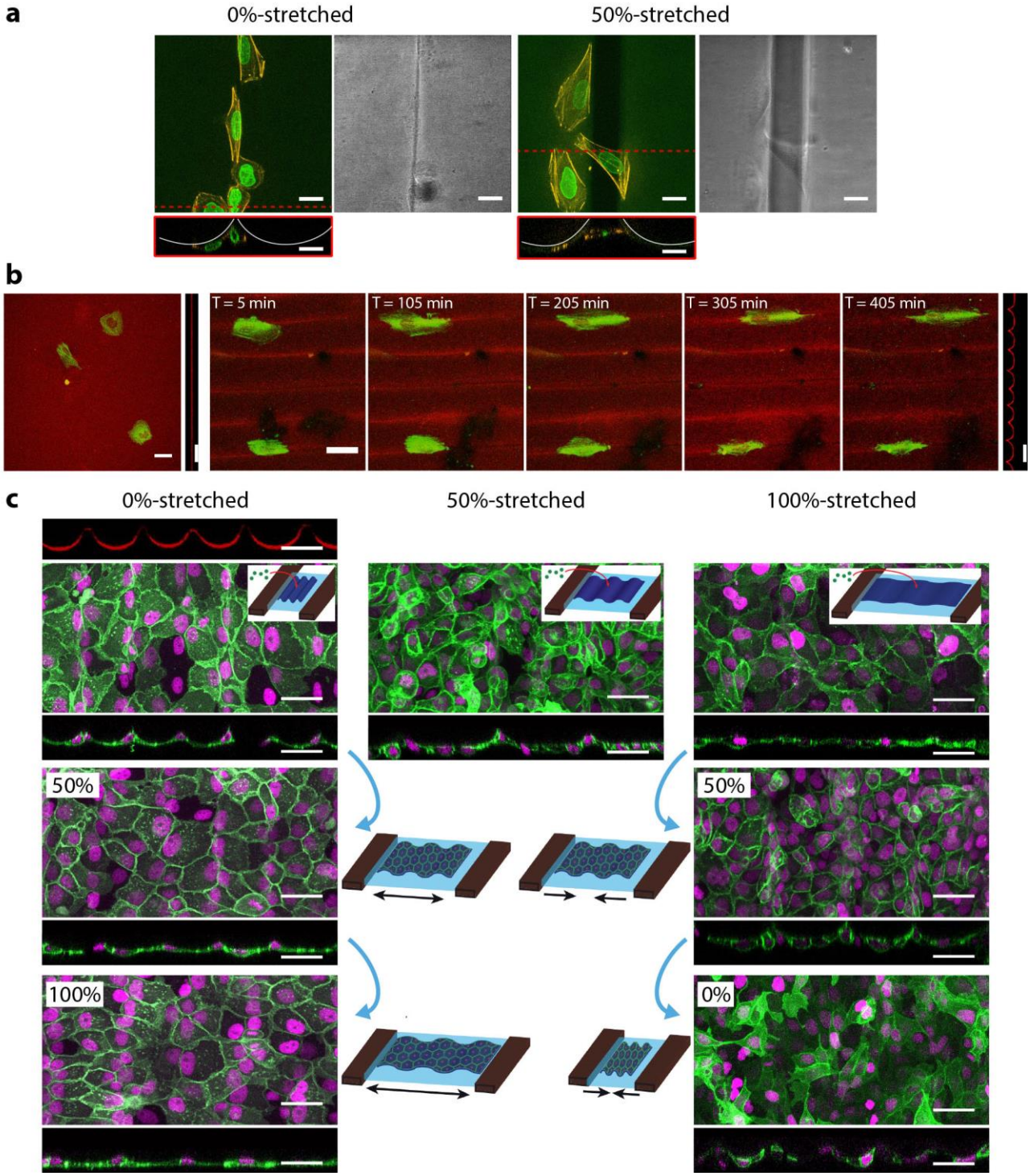

Figure 6. **Single and multi-cell adaptation to homogeneous wrinkled patterns.** a) Hela cells on non-stretched and 50% stretched substrates. Maximum-intensity projections of 3D confocal images (left) with cross-sections along the dashed red line (bottom) and bright-field image (right). The white lines in the cross-sections highlight the wrinkle profiles. Actin (SiR-Actin, orange), nuclei (green, LaminB1, green). Scale bars = 20 µm. b) Saos-2 cells on a flat 100% stretched substrate then relaxed to the initial position. Cross-sections show the flat substrate and the wrinkles formed after relaxation. "T" indicates time (in minutes) after relaxation. Fibronectin (red), actin (mEGFP-Lifeact-7, green). Scale bars = 40 µm. c) Top views and orthogonal sections of MDCK cells at different rates of substrate stretching: 0% (relaxed), 50% and 100%. Top: cells adhere on the three static configurations. Left, from top to bottom: cells are seeded on a relaxed substrate and then stretched to 50% and 100%. Right, from top to bottom: cells are seeded on a 100% stretched substrate and then compressed to 50% and 0%. Fibronectin (red), cell membrane (Myr-Palm-GFP, green), nuclei (H2B-mCherry, magenta). Scale bars = 40 µm.

In the present paper, the wrinkled morphologies created by the laser irradiation approach were explored for guiding living cell motility and shape. Indeed, the biocompatibility, the transparency, and the low thickness of the elastomer film make this substrate ideal for biological observations. The mid-infrared laser exposure approach provides high flexibility of the film and high resistance to irregular cracks on the surface, which are especially adapted properties for periodic and dynamic deformations of the substrate. Moreover, this quality is particularly important for cell cultures, also in order to avoid uncontrolled sub-cellular topographies. The bigger size of the wrinkled morphology obtained by this approach gives the opportunity to reproduce cell-scale curved substrates. We showed that cells have the ability to sense substrate curvature (curvotaxis) from single cell scale to multicellular level. On one side, we observed an active adaptation of cell orientation and migration along the wrinkled substrates. On the other side, we showed how cells can be passively deformed in space and time by modulating the substrate stretching, and therefore the wrinkled morphology. Finally, we explored other 3D structured films made by laser irradiation, whose optimization may lead to new deformable cell environments. We hope that the present work will inspire further studies on cell migration and cell fate determination controlled by curvature.

6. Experimental Section

Laser Treatment for Wrinkles Formation: A silicone elastomer film (Silex Ltd, Linford, UK, super clear sheet, 0.5 mm thick, #HT6240 40SH) was exposed with a laser beam (Gravotech, Rillieux-la-Pape, France, LS100 laser). The prestress of the film was performed using a homemade stretcher, allowing an elongation up to 100% of the film length. The typical irradiation dose was estimated by irradiating a rectangle having the surface S = 10 cm^2. At the relative scan velocity 20%, irradiation takes t = 33 s. Then the dose can be calculated as $A = \frac{fPt}{S} = 23.1\ J\ cm^{-2}$, where f = 0.2 is the relative power of the laser, and P = 35 W is the maximal power.

Cell Culture and Staining: Hela Kyoto enhanced green fluorescent protein (EGFP)-LaminB1/H2B-mCherry cells (Cell Lines Service (CLS) GmbH, Eppelheim, Germany, #330919), MDCK cells, and Saos-2 cells were used. The cell growing medium for Hela cells was: Dulbecco's modified Eagle medium (DMEM, Thermo Fisher Scientific, Waltham, USA, Cat. No. 31966021) supplemented with 10% fetal bovine serum (FBS, Thermo Fisher Scientific, Waltham, USA, Cat. No. 102701036), 1% of penicillin-streptomycin (PS, Thermo Fisher Scientific, Waltham, USA, Cat. No. 15140122), 0.5 mg mL−1 of Geneticin G418 (BioConcept AG, Allschwill, Switzerland Cat. No. 4-15F01-H), and 0.5 µg mL^{-1} of puromycin (Thermo Fisher Scientific, Waltham, Cat. No. A11138-03). The MDCK cells medium was: DMEM (Thermo Fisher Scientific, Waltham, USA, Cat. No. 61965026) supplemented with 10% FBS, 1% of PS and 1% of nonessential amino acids solution (Thermo Fisher Scientific, Waltham, USA, Cat. No. 11140035). The Saos-2 cells medium was: McCoy's 5a Medium Modified supplemented (Sigma Aldrich, St. Louis, USA) with 10% FBS (Biowest, Nuaillé, France, Cat. No. S182H-100), 1% of PS.

Chemical dissociation of cells was carried out by incubation in trypsinethylenediaminetetraacetic acid (EDTA) 0.05% (Thermo Fisher Scientific, Waltham, USA, Cat. No. 25300054) for 5 min at 37 °C. Cells were then seeded on the elastomer films that were coated with fibronectin (3 µg cm^{-2}, 1 h incubation in phosphate-buffered saline (PBS) at 37 °C after oxygen plasma activation for 30 s, Life Technologies, USA, Cat. No. 33016015) at 20 000 cells per cm2 and incubated in a humidified atmosphere at 37 °C and 5% CO_2. The cell solution was maintained on the wrinkled surface by a PDMS well attached to the elastomer film with a biocompatible glue (Picodent, Wipperfurth, Germany). After about 4 h, samples were washed with fresh growing medium in order to remove nonadhesive cells and maintained in culture to allow cell monolayer formation (in the case of MDCK cells). Then, when Hela or Saos-2 cells were used, the medium was replaced by medium for live imaging observations (growing medium without phenol red, MEM, Thermo Fisher Scientific, Waltham, USA, Cat. No. 51200046). 1 h before imaging, for Hela cells, F-Actin was stained with SiR-Actin (1 × 10^{-6} m dilution, Spirochrome, Stein am Rhein, Switzerland, Cat. No. SC-001); Saos-2 cells were transfected with monomeric enhanced green fluorescent protein (mEGFP)-Lifeact-7 from Addgene for actin following the instructions of the manufacturer of Lipofectamine 3000 (Thermo Fisher Scientific, lot 1857477). mEGFP-Lifeact-7 was a gift from Michael Davidson (Addgene plasmid No. 54610; http://n2t.net/ addgene:54610; RRID:Addgene_54610).

The cell line MDCK Myr-Palm-GFP, a kind gift from the lab of Dr. Mathieu Piel (Institut Curie, Paris, France), was used to generate the cell line MDCK Myr-Palm-GFP H2B-mCherry. The plasmid H2BmCherry, a gift from Robert Benezra (Addgene plasmid No. 20972), was inserted into the pLenti6.3/V5-DEST vector (containing C-terminal mCherry) using the Gateway cloning system. Lentiviral particles were generated in HEK293T cells using third generation lentiviral packaging vectors and MDCK Myr-Palm-GFP cells were infected with pLenti-H2BmCherry. After infection, cell clones expressing both markers were sorted by fluorescence activated cell sorting using a Beckman Coulter MoFlo Astrios, and monoclonal cells with unchanged morphology and sufficient expression level of the transgenes was selected.

Cell lines were tested negative for contamination with mycoplasma (Eurofins GATC Biotech, Germany).

Surface Characterization: The topography characterization of the wrinkled surfaces was performed with three different techniques: SEM (FEI Quanta 400, tungsten gun); digital microscope (Olympus DSX 510); and confocal

microscopy. For the latter technique, the surface was made fluorescent by labeling the protein coating (Rhodamin Fibronectin, 3 μg cm^{-2}, 1 h incubation in PBS at Room Temperature, Cytoskeleton, Inc., Denver, USA, Cat. No. FNR01) or it was extracted by the negative image of the fluorescent medium (fluorescein isothiocyanate-dextran 70 000 MW, Sigma, Lot BCBP1019V).
Spectroscopic measurements were performed on a Nicolet IS 50 FTIR spectrometer (Thermo Scientific Fisher, USA) coupled with an ATR accessory (Smart OMNI-Sampler Germanium ATR Sampling Accessory). Spectra were collected at wavenumbers ranging from 650 to 4000 cm^{-1}, with a resolution of 4 cm^{-1} and 64 scans. Background spectra collected on blank ATR spectra were automatically subtracted. For each sample, five replicates were collected to produce a unique spectrum in order to eliminate loading errors. Peak's area were calculated in a range between 950–1150, 750–850, and 1200–1300 cm−1, respectively, for stretching motion "ν" of the siloxane group, rocking "ρ" vibrations, and symmetric bending "δs" vibrations for the methyl group.
Confocal and Live Imaging: Confocal images were obtained using an upright LSM 700 with W-Plan-Apochromat 20x/1.0 differential interference contrast (DIC) objective (Carl Zeiss). An upright LSM 710 microscope with a Plan-Apochromat 20x/1.0 DIC objective (Carl Zeiss) was used to get confocal images of the MDCK and Hela cells on the wrinkled surface on the stretcher device. Live imaging of Hela cells for cell tracking on the wrinkled surfaces was performed with an LSM 780 microscope with a 10x and 20x/1.0 DIC objectives (Carl Zeiss) with controlled environment (37 °C, 5% CO2).
Data Collection and Analysis: Image analysis was performed with ImageJ (TrackMate plugin for nucleus tracking analysis[50]), Zen (for fibronectin coating profiles), Imaris (segmentation of nuclei and cells, respectively, with the Spots and Cells packages, for orientation and aspect ratio analyses), and Matlab (analyses of track orientations and nucleus speed). Unless otherwise stated in the figure legend, data are expressed as the mean ± standard deviation (s.d.). All sample numbers and the *p*-values are reported in the figure legends. *P*-values >0.5 were considered as not significant (ns). Each experiment was repeated at least three times. All statistical tests were performed using Prism software (GraphPad). Since data distributions were not following normality assumptions, nonparametric tests were used (Mann–Whitney, two-tailed).

Supporting Information
Supporting Information is available from the Wiley Online Library or from the author.

Acknowledgements
The authors thank the IS2M facilities platform for their technical support, in particular Stephen Knopf for SEM, Simon Gree for Raman spectroscopy, and FT-IR and Philippe Kunemann for Digital Microscope. Authors also thank the Bioimaging Center and Nicolas Liaudet from the Bioimaging Core Facility of University of Geneva for their technical support and Pau Guillamat for valuable discussions and support for the data analysis performed with Matlab. This work was partially supported by the French National Research Agency ANR- 17-CE18-0031-01. A.R. acknowledges funding from the SystemsX EpiPhysX consortium, the Human Frontier Science Program Young Investigator Grant RGY0076/2009-C, the Swiss National Fund for Research Grants N°31003A_130520, N°31003A_149975 and N°31003A_173087, and the European Research Council Consolidator Grant No. 311536. I.D.M. and A.R. acknowledge funding from Secrétariat d'Etat à la Recherche et à l'Innovation grant agreement REF-1131-52107 and from the EU Horizon2020 Marie Sklodowska- Curie ITN "BIOPOL" (Grant Agreement No. 641639).

Conflict of Interest
The authors declare no conflict of interest.

Keywords
cell curvotaxis, curvature, dynamic substrates, laser treatment, strain engineering

Received: January 10, 2019
Revised: March 1, 2019
Published online: April 5, 2019

References
[1] A. M. Ross, Z. Jiang, M. Bastmeyer, J. Lahann, *Small* **2012**, *8*, 336.
[2] M. Ermis, E. Antmen, V. Hasirci, *Bioact. Mater.* **2018**, *3*, 355.
[3] G. Halder, S. Dupont, S. Piccolo, *Nat. Rev. Mol. Cell Biol.* **2012**, *13*, 591.
[4] M. Versaevel, T. Grevesse, S. Gabriele, *Nat. Commun.* **2012**, *3*, 671.

[5] L. Pieuchot, J. Marteau, A. Guignandon, T. Dos Santos, I. Brigaud, P. F. Chauvy, T. Cloatre, A. Ponche, T. Petithory, P. Rougerie, M. Vassaux, J. L. Milan, N. Tusamda Wakhloo, A. Spangenberg, M. Bigerelle, K. Anselme, *Nat. Commun.* **2018**, *9*.
[6] J. Swift, I. L. Ivanovska, A. Buxboim, T. Harada, P. D. P. Dingal, J. Pinter, J. D. Pajerowski, K. R. Spinler, J. W. Shin, M. Tewari, F. Rehfeldt, *Science (80-.).* **2013**, *341*, 1240104.
[7] C. Guilluy, L. D. Osborne, L. Van Landeghem, L. Sharek, R. Superfine, R. Garcia-Mata, K. Burridge, *Nat. Cell Biol.* **2014**, *16*, 376.
[8] C. Schwartz, M. Fischer, K. Mamchaoui, A. Bigot, T. Lok, C. Verdier, A. Duperray, R. Michel, I. Holt, T. Voit, S. Quijano-Roy, G. Bonne, C. Coirault, *Sci. Rep.* **2017**, *7*, 1.
[9] V. Yakovlevich Prinz, V. Alexandrovich Seleznev, A. Victorovich Prinz, A. Vladimirovich Kopylov, *Sci. Technol. Adv. Mater.* **2009**, *10*.
[10] V. Luchnikov, O. Sydorenko, M. Stamm, *Adv. Mater.* **2005**, *17*, 1177.
[11] V. Luchnikov, L. Lonov, M. Stamm, *Macromol. Rapid Commun.* **2011**, *32*, 1943.
[12] Y. Ma, K. I. Jang, L. Wang, H. N. Jung, J. W. Kwak, Y. Xue, H. Chen, Y. Yang, D. Shi, X. Feng, J. A. Rogers, Y. Huang, *Adv. Funct. Mater.* **2016**, *26*, 5345.
[13] W. T. S. Huck, N. Bowden, P. Onck, T. Pardoen, J. W. Hutchinson, G. M. Whitesides, *Langmuir* **2000**, *16*, 3497.
[14] X. Jiang, S. Takayama, X. Qian, E. Ostuni, H. Wu, N. Bowden, P. LeDuc, D. E. Ingber, G. M. Whitesides, *Langmuir* **2002**, *18*, 3273.
[15] A. Chen, D. K. Lieu, L. Freschauf, V. Lew, H. Sharma, J. Wang, D. Nguyen, I. Karakikes, R. J. Hajjar, A. Gopinathan, E. Botvinick, C. C. Fowlkes, R. A. Li, M. Khine, *Adv. Mater.* **2011**, *23*, 5785.
[16] Q. Zhou, O. C. Ocampo, C. F. Guimarães, P. T. Kühn, T. G. van Kooten, P. van Rijn, *ACS Appl. Mater. Interfaces* **2017**, *9*, 31433.
[17] H. Izawa, N. Okuda, T. Yonemura, K. Kuroda, K. Ochi, S. Ifuku, M. Morimoto, H. Saimoto, M. Noda, K. Azuma, Y. Okamoto, *Colloids and Interfaces* **2018**, *2*, 15.
[18] D. S. Kim, H. W. Lee, J. H. Lee, H. G. Kwon, S. W. Lee, S. J. Han, O. C. Jeong, *Colloids Surfaces B Biointerfaces* **2018**, *170*, 266.
[19] A. K. Epstein, D. Hong, P. Kim, A. Joanna, *New J. Phys.* **2013**, *15*, 095018.
[20] J. I. Luna, J. Ciriza, M. E. Garcia-Ojeda, M. Kong, A. Herren, D. K. Lieu, R. A. Li, C. C. Fowlkes, M. Khine, K. E. McCloskey, *Tissue Eng. Part C Methods* **2011**, *17*, 579.
[21] C. M. Stafford, C. Harrison, K. L. Beers, A. Karim, E. J. Amis, M. R. VanLandingham, H.-C. Kim, W. Volksen, R. D. Miller, E. E. Simonyi, *Nat. Mater.* **2004**, *3*, 545.
[22] E. A. Wilder, S. Guo, S. Lin-Gibson, M. J. Fasolka, C. M. Stafford, *Macromolecules* **2006**, *39*, 4138.
[23] E. P. Chan, E. J. Smith, R. C. Hayward, A. J. Crosby, *Adv. Mater.* **2008**, *20*, 711.
[24] C. Harrison, C. M. Stafford, W. Zhang, A. Karim, *Appl. Phys. Lett.* **2004**, *85*, 4016.
[25] H. Guo, J. Tang, K. Qian, D. Tsoukalas, M. Zhao, J. Yang, B. Zhang, X. Chou, J. Liu, C. Xue, W. Zhang, *Sci. Rep.* **2016**, *6*, 1.
[26] Y. Wang, C. Zhu, R. Pfattner, H. Yan, L. Jin, S. Chen, F. Molina-Lopez, F. Lissel, J. Liu, N. I. Rabiah, Z. Chen, J. W. Chung, C. Linder, M. F. Toney, B. Murmann, Z. Bao, *Sci. Adv.* **2017**, *3*, e1602076.
[27] J. Tang, H. Guo, M. Zhao, J. Yang, D. Tsoukalas, B. Zhang, J. Liu, C. Xue, W. Zhang, *Sci. Rep.* **2015**, *5*, 1.
[28] D. Maji, D. Das, J. Wala, S. Das, *Sci. Rep.* **2015**, *5*, 1.
[29] M. Werner, N. A. Kurniawan, G. Korus, C. V. C. Bouten, A. Petersen, *J. R. Soc. Interface* **2018**, *15*, 16.
[30] K. E. Broaders, A. E. Cerchiari, Z. J. Gartner, *Integr. Biol.* **2015**, *7*, 1611.
[31] K. Efimenko, M. Rackaitis, E. Manias, A. Vaziri, L. Mahadevan, J. Genzer, *Nat. Mater.* **2005**, *4*, 293.
[32] W. Pabst, E. Gregorová, *Ceramics-Silikaty* **2013**, *57*, 167.
[33] J. Y. Chung, A. J. Nolte, C. M. Stafford, *Adv. Mater.* **2011**, *23*, 349.
[34] Y. Ma, Y. Xue, K.-I. Jang, X. Feng, J. A. Rogers, H. Yonggang, *Proc. R. Soc. A Math. Phys. Eng. Sci.* **2016**, *472*, 20160339.
[35] Z. Y. Huang, W. Hong, Z. Suo, *J. Mech. Phys. Solids* **2005**, *53*, 2101.
[36] F. Brau, P. Damman, H. Diamant, T. A. Witten, *Soft Matter* **2013**, *9*, 8177.
[37] L. D. Landau, E. M. Lifshitz, *Theory of Elasticity*; Third Edit.; Pergamon: NY, 1986.
[38] H. Fei, H. Jiang, D.-Y. Khang, *J. Vac. Sci. Technol. A Vacuum, Surfaces, Film.* **2009**, *27*, L9.
[39] N. E. Stankova, P. A. Atanasov, R. G. Nikov, R. G. Nikov, N. N. Nedyalkov, T. R. Stoyanchov, N. Fukata, K. N. Kolev, E. I. Valova, J. S. Georgieva, S. A. Armyanov, *Appl. Surf. Sci.* **2016**, *374*, 96.
[40] T. Deschaines, J. Hodkiewicz, P. Henson, *ThermoFisher Appl. Note 51735* **2009**, 3.
[41] P. A. Atanasov, N. E. Stankova, N. N. Nedyalkov, N. Fukata, D. Hirsch, B. Rauschenbach, S. Amoruso, X. Wang, K. N. Kolev, E. I. Valova, J. S. Georgieva, S. A. Armyanov, *Appl. Surf. Sci.* **2016**, *374*, 229.
[42] D. A. Long, *Infrared and Raman characteristic group frequencies. Tables and charts*; Third Edit.; George Socrates John Wiley and Sons, Ltd, Chichester, 2004; Vol. 35.

[43] C. Camino, S. M. Lomakin, M. Lazzari, *Polymer (Guildf).* **2001**, *42*, 2395.
[44] G. Camino, S. M. Lomakin, M. Lageard, *Polymer (Guildf).* **2002**, *43*, 2011.
[45] S. Timoshenko, *J. Opt. Soc. Am.* **1925**, *11*, 233.
[46] M. L. Dano, M. W. Hyer, *Int. J. Solids Struct.* **2003**, *40*, 5949.
[47] S. Daynes, C. G. Diaconu, K. D. Potter, P.M. Weaver, *J. Compos. Mater.* **2010**, *44*, 1119.
[48] H. Shao, S. Wei, X. Jiang, D. P. Holmes, T. K. Ghosh, *Adv. Funct. Mater.* **2018**, *28*, 1.
[49] D. Yu, H. Wensheng, G. Zhongning, H. Zhigang, C. Ying, *Procedia CIRP* **2018**, *68*, 168.
[50] J. Y. Tinevez, N. Perry, J. Schindelin, G. M. Hoopes, G. D. Reynolds, E. Laplantine, S. Y. Bednarek, S. L. Shorte, K. W. Eliceiri, *Methods* **2017**, *115*, 80.